How grain boundaries limit supercurrents in high-temperature superconductors

S. Graser,[1,2,*] P. J. Hirschfeld,[2] T. Kopp,[1] R. Gutser,[1] B. M. Andersen,[3] and J. Mannhart[1]

[1]*Center for Electronic Correlations and Magnetism, Institute of Physics, University of Augsburg, D-86135 Augsburg, Germany*

[2]*Department of Physics, University of Florida, Gainesville, FL 32611, USA*

[3]*Niels Bohr Institute, University of Copenhagen, Universitetsparken 5, DK-2100 Copenhagen, Denmark*

(Dated: April 12, 2010)

The interface properties of high-temperature cuprate superconductors have been of interest for many years, and play an essential role in Josephson junctions, superconducting cables, and microwave electronics. In particular, the maximum critical current achievable in high-T_c wires and tapes is well known to be limited by the presence of grain boundaries, regions of mismatch between crystallites with misoriented crystalline axes. In studies of single, artificially fabricated grain boundaries the striking observation has been made that the critical current J_c of a grain boundary junction depends *exponentially* on the misorientation angle. Until now microscopic understanding of this apparently universal behavior has been lacking. We present here the results of a microscopic evaluation based on a construction of fully 3D $YBa_2Cu_3O_{7-\delta}$ grain boundaries by molecular dynamics. With these structures, we calculate an effective tight-binding Hamiltonian for the d-wave superconductor with a grain boundary. The critical current is then shown to follow an exponential suppression with grain boundary angle α. We identify the buildup of charge inhomogeneities as the dominant mechanism for the suppression of the supercurrent.

To explain the exponential dependence of the critical current J_c on the misorientation angle[1,2] Chaudhari and collaborators[3] introduced several effects which can influence the critical current that are particular to high-temperature superconductor (HTS) grain boundaries (GB). First, a variation with angle can arise from the relative orientation of the d-wave order parameters pinned to the crystal lattices on either side of the boundary. This scenario was investigated in detail by Sigrist and Rice[4] and by Yokoyama *et al.*[5]. However, such a modelling cannot explain the exponential suppression of the critical current over the full range of misorientation angles. Secondly, dislocation cores, whose density grows with increasing angle, can suppress the total current. A model assuming insulating dislocation cores which nucleate antiferromagnetic regions and destroy superconducting order was studied by Gurevich and Pashitskii[6]. However, for grain boundary angles beyond approximately 10° when the cores start to overlap such model does not apply. Finally, variations of the stoichiometry in the grain boundary region, such as in the oxygen concentration, may affect the scattering of carriers and consequently the critical current. Stolbov and collaborators[7] as well as Pennycook and collaborators[8] have examined the bond length distribution near the grain boundary and calculated the change in the density of states at the Fermi level, or

the change in the Cu valence, respectively. In the latter work the authors used the reduced valences to define an effective barrier near the boundary whose width grows linearly with misorientation angle.

A critical examination of the existing models shows that the difficulty of the longstanding HTS "grain boundary problem" arises from the multiple length scales involved: atomic scale reconstruction of the interface, the electrostatic screening length, the antiferromagnetic correlation length, and the coherence length of the superconductor. Thus it seems likely that only an approach that carefully balances these competing lengthscales can succeed.

Our goal in this paper is to simulate, in the most realistic way possible, the nature of the actual grain boundary in a cuprate HTS system, in order to characterize the multiple scales which cause the exponential suppression of the angle dependent critical current. To achieve this goal we proceed in a stepwise fashion, first simulating the atomic structure of realistic YBCO grain boundaries and assuring ourselves that our simulations are robust and duplicate the systematics of actual grain boundaries. Subsequently we construct an effective disordered tight-binding model, including d-wave pairing, whose parameters depend on the structures of the simulated grain boundaries in a well-defined way. Thus for any angle it will be possible to calculate the critical current; then, for a given pairing amplitude (reasonably well known from experiments on bulk systems) the form of $J_c(\alpha)$ and its absolute magnitude is calculated. Here we emphasize that the physics arising from surface Andreev bound states, which are known to have a decisive influence on the Josephson currents[10–15], is completely included in the model, although we do not analyze it in detail.

We simulate YBCO grain boundaries by a molecular dynamics (MD) procedure which has been shown to reproduce the correct structure and lattice parameters of the bulk $YBa_2Cu_3O_{7-\delta}$ crystal[16], and adapt techniques which were successfully applied to twist grain boundaries in monocomponent solids[17]. We only sketch the procedure here, and postpone its details to the supplementary information and a longer publication. The method uses an energy functional within the canonical ensemble

$$H = \frac{1}{2}\sum_{i=1}^{N}\sum_{\alpha=1}^{3} m_i \dot{r}_{i,\alpha}^2 + \frac{1}{2}\sum_{i=1}^{N}\sum_{j=1,j\neq i}^{N} U(r_{ij}), \tag{1}$$

where m_i is the mass of the ion and $U(r_{ij})$ is the effective potential between ions, taken to be of the form $U(r_{ij}) = \Phi(r_{ij}) + V(r_{ij})$. Here $V(r)$ is the screened Coulomb interaction $V(r) = \pm e^{-\kappa r} Z^2 e^2/(4\pi\epsilon_0 r)$ with screening length κ^{-1}, and $\Phi(r)$ is a short range Buckingham

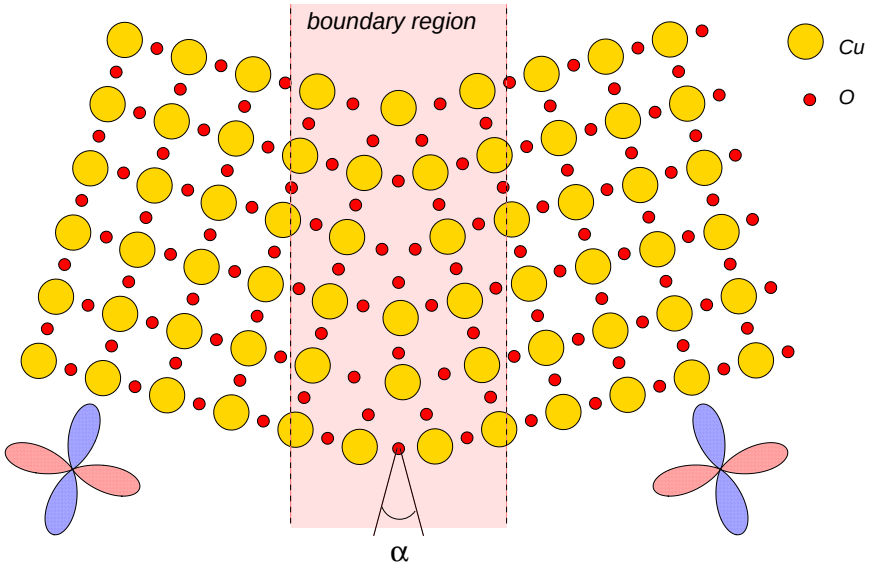

Figure 1: **Schematic of an HTS symmetric grain boundary.** The misorientation angle α and the orientation of the d-wave order parameters are indicated.

potential $\Phi(r) = A\exp(-r/\rho) - C/r^6$. We take the parameters A, ρ and C from Ref. 16, and the initial lattice constants are $a = 3.82$ Å, $b = 3.89$ Å and $c = 11.68$ Å. To construct a grain boundary with well defined misorientation angle, we must fix the ion positions on both sides far from the boundary, and ensure that we have a periodic lattice structure along the grain boundary and also along the c-axis direction. Therefore we apply periodic boundary conditions in the molecular dynamics procedure in the direction parallel to the GB and also in the c-axis direction. In the direction perpendicular to the GB only atomic positions with a distance smaller than six lattice constants from the GB are reconstructed. This method restricts our consideration to grain boundary angles that allow a commensurate structure parallel to the GB, e.g. angles $\alpha = 2 \cdot \arctan[N_1 a/(N_2 b)]$, $N_1, N_2 \in \mathbf{N}$. In the following we will call a GB with $N_1 = 1$, $N_2 = 4$ and therefore a GB angle of $\alpha = 2 \cdot 0.24074$ rad $= 27.58°$ a symmetric (410) GB.

An important step to be taken before starting the reconstruction of the GB is the initial preparation of the GB. Since we use a fixed number of ions at the GB within the molecular dynamics algorithm we have to initialize it with the correct number of ions. If we start with two perfect but rotated crystals on both sides of the interface, in which all ions in the half space behind the imaginary boundary line are cut away, we find that several ions are unfavorably close to each other. Here we have to use a set of selection rules to replace two

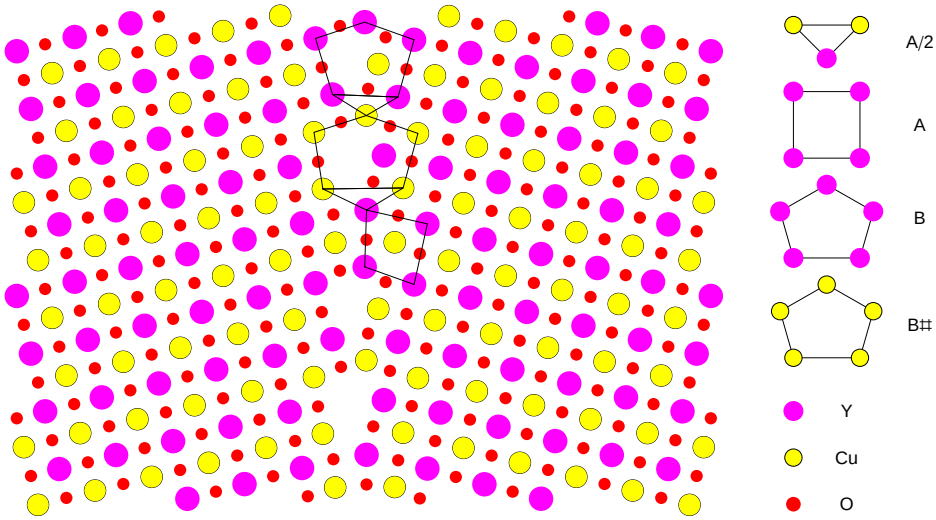

Figure 2: **Top view of a calculated (410) grain boundary.** Here only the Y and the CuO_2 layers are shown. The dots show the position of Y ions (magenta), Cu ions (yellow), and O ions (red). Structural units are indicated by solid black lines. For this particular angle we find a sequence of the form A(A/2)B#(A/2)B, in agreement with the experimental results given in Table 1 of Ref. 8 (for notation see this reference).

ions by a single one at the grain boundary. These selection rules have to be carefully chosen for each type of ion since they determine how many ions of each type are present in the grain boundary region; the rules are detailed in the supplementary information. Ultimately they should be confirmed by a grand canonical MD procedure. However, such a procedure for a complex multicomponent system as the YBCO GB is technically still not feasible. While the selection rules are *ad hoc* in nature, we emphasize that they are independent of misorientation angle, and reproduce correctly the stoichiometry of Cu, Y, and O ions found for comparable GB angles in TEM studies.[8].

With the initial conditions established, the MD equations of motion associated with Eq. 1 are iterated until all atoms are in equilibrium. As an example, we show in Fig. 2 the reconstructed positions of Y, Cu, and O ions for a (410) boundary. We emphasize that the MD simulation is performed for *all* the ions in the YBCO full 3D unit cells of two misoriented crystals except for a narrow "frame" consisting of ions that are fixed to preserve the crystalline order far from the grain boundary. The sequence of typical structural units

identified in the experiments[8] is also indicated and we find excellent agreement.

We next proceed to construct an effective tight-binding model which is restricted to the Cu sites, the positions of which were determined through the algorithm described. We calculate hopping matrix elements t_{ij} of charge carriers (holes) up to next nearest neighbor positions of Cu ions. The Slater-Koster method is used to calculate the directional dependent orbital overlaps of Cu-3d and O-2p orbitals[18,19]. The effective hopping between Cu positions is a sum of direct orbital overlaps and hopping via intermediate O sites, where the latter is calculated in 2nd order perturbation theory. For the homogeneous lattice, these parameters agree reasonably well with the numbers typically used in the literature for YBCO. Exact values and details of the procedure are given in the supplementary information. Results for a (410) grain boundary are shown in Fig. 3. Note the largest hopping probabilities across the grain boundary are associated with the 3fold coordinated Cu ions which are close to dislocation cores. The inhomogeneities introduced through the distribution of hopping probabilities along the boundary induce scattering processes of the charge carriers and consequently contribute to an "effective barrier" at the grain boundary. We note that the angular dependence of the critical current $J_c(\alpha)$ is not directly related to the changes in averaged hopping parameters observed for different misalignment angles. In fact we found that the variation of the hopping probabilities with boundary angle cannot account by itself for the exponential dependence of $J_c(\alpha)$ over the whole range of misalignment angles.

The structural imperfection at the grain boundary will necessarily lead to charge inhomogeneities that will contribute—in a similar way as the reduced hopping probabilities—to the effective barrier that blocks the superconducting current over the grain boundary. We include these charge inhomogeneities into the calculations by considering them in the effective Hamiltonian as on-site potentials on the Cu sites. To accomplish this we utilize the method of valence bond sums. The basic idea is to calculate the bond valence of a cation by

$$V_i = \sum_j \exp\left(\frac{r_0 - r_{ij}}{B}\right) \tag{2}$$

where j runs over all neighboring anions, in our case the neighboring negatively charged oxygen ions. The parameter $B = 0.37$ Å is a universal constant in the bond valence theory, while r_0 is different for all cation-anion pairs and also depends on the formal integer oxidation state of the cation (the values are listed in Ref. 23). Strong deviations from the formal valence

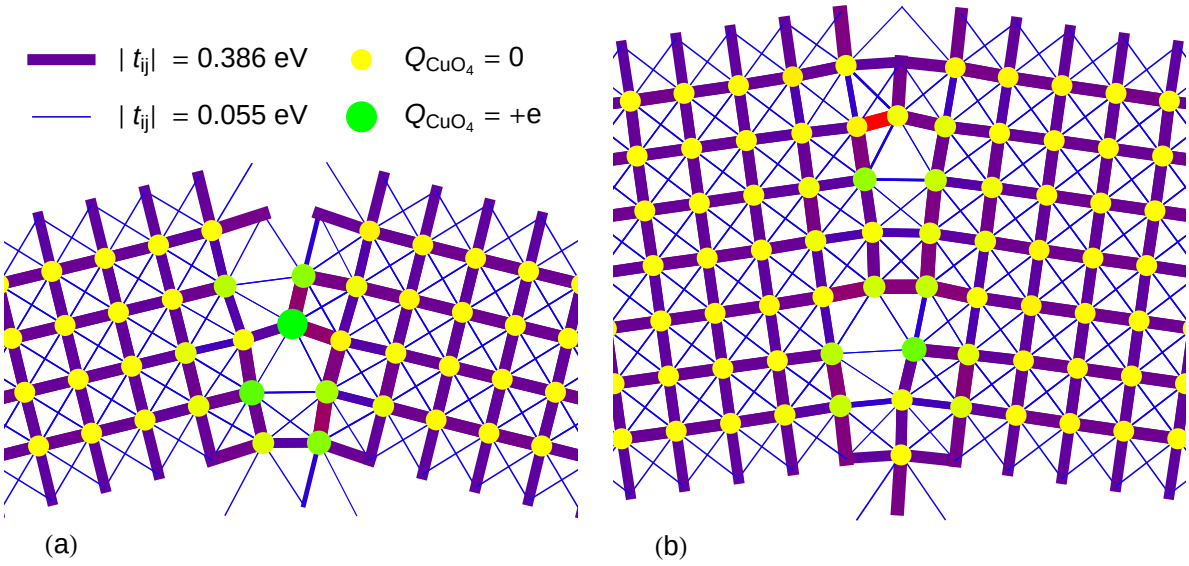

Figure 3: **Tight-binding model for the CuO_2 plane.** Hopping values between the Cu ions calculated from the interatomic matrix elements for a (410) grain boundary (a) and for a (710) grain boundary (b). The line thickness and line colors characterize the hopping amplitudes (blue: weak, red: strong) and the color and size of the copper sites illustrate the on-site potential.

reveal strain or even an incorrect structure. This procedure is straightforward in the case of the Y^{3+} and Ba^{2+} ions, while it is slightly more complicated for the Cu ions, because they have more than one formal integer oxidation state[22,23]. We show in Fig. 4 the distribution of charges at the (410) grain boundary obtained. We also calculate by similar methods the oxidation state of the oxygen ions. Here, charge neutrality is ensured because the already determined cation valences are used.

In the next step we account for the effect of broken Cu-O bonds at the grain boundary that give rise to strong changes of the electronic configuration of the Cu atoms as well as of the electronic screening of charges, as shown in first principle calculations[7]. Unfortunately there is no straightforward way to include these changes in the electronic configuration into a purely Cu-based tight-binding Hamiltonian. On the other hand we know that the additional holes doped into the CuO_2 planes form Zhang-Rice singlets residing on a CuO_4 square rather than on a single Cu site[24], and are therefore affected not only by the charge of the Cu ion but also by the charge of the surrounding oxygens. Modelling this situation, we use a phenomenological potential to sum the Cu and the O charges to obtain an effective

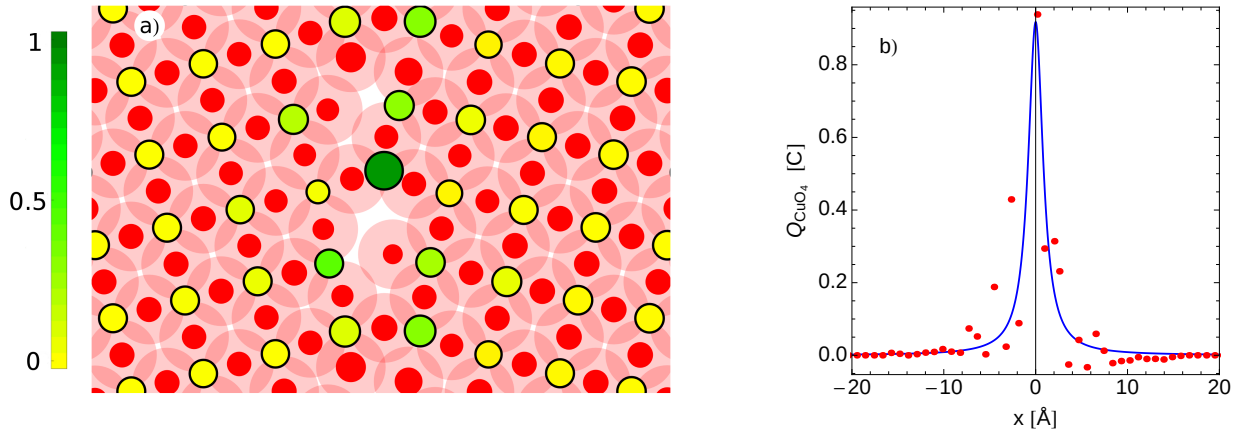

Figure 4: **Charging of the CuO_4 squares.** a) Charge distribution on copper (yellow/green) and oxygen (red) sites at a 410 boundary. The diameter of the circles is a measure for positive (copper) or negative (oxygen) charge, as determined by the bond valence analysis. The color of the copper sites represents the charging of the corresponding CuO_4 squares as described by Eq. 3, with green circles referring to a positive charge compared to the bulk charge (see color scale). The transparent red circles represent the oxygen contributions to the CuO_4 charge. b) Plot of average charge on squares vs. distance from grain boundary (red points), and fit by a Lorentzian (blue line).

charge of the CuO_4 square. This effective charge is taken as

$$Q_{\mathrm{CuO_4}}(i) = Q_{\mathrm{Cu}}(i) + A \sum_j Q_0(j) e^{-r_{ij}^2/\lambda^2}, \tag{3}$$

where A and λ are two constants chosen to yield a neutral Cu site if 4 oxygen atoms are close to the average Cu-O distance. Correspondingly, the energy cost of a Cu site that has only 3 close oxygen neighbors instead of all 4 neighbors, is strongly enhanced. Thus, the broken Cu-O bonds induce strong charge inhomogeneities in the "void" regions of the grain boundary, mainly described by pentagonal structural units, while Cu sites belonging to "bridge" regions with mostly quadrangular structural units have charge values close to their bulk values.

Finally we have to translate the effective fractional charge on the Cu sites (or better CuO_4 squares) into effective on-site lattice potentials. The values of screening lengths in the cuprates, and particularly near grain boundaries, are not precisely known, but near optimal doping they are of order of a lattice spacing or less. We adopt a mean field approach and assume a 3D Yukawa-type screening with phenomenological length parameter ℓ of this order,

and find a potential integrated over a unit cell V_0 of

$$\frac{V_0}{a^2\bar{q}} \approx 4\pi\ (a_0\ell)\ \text{Ryd} \approx 10\ \text{eV}, \tag{4}$$

where $\bar{q}$ is the charge in units of the elementary charge, a_0 is the Bohr radius, and ℓ is taken to be 2 Å while $a = 4$ Å. Thus we find a surplus charge of a single elementary charge integrated over a unit cell to produce an effective potential of around 10 eV. In the following we will use an effective potential of either 6 or 10 eV per elementary charge, reflecting the uncertainty in this parameter. The value of the effective potential will affect the scale of the final critical current.

To calculate the order parameter profile and the current across the grain boundary we solve the Bogoliubov-de Gennes mean field equations of inhomogeneous superconductivity self-consistently. The Hamiltonian is

$$\hat{H} = \sum_i \epsilon_i \hat{n}_{i\sigma} - \sum_{ij\sigma} t_{ij}\hat{c}^\dagger_{i\sigma}\hat{c}_{j\sigma} + \sum_{ij}\left(\Delta_{ij}\hat{c}^\dagger_{i\uparrow}\hat{c}^\dagger_{j\downarrow} + \text{h.c.}\right), \tag{5}$$

where the effective hopping parameters t_{ij} are determined for a given grain boundary by the procedure described above and the onsite energies $\epsilon_i = u_i - \mu$ are a sum of the effective charge potentials $u_i = (V/Q)q_i$ with $V/Q = 6(10)$eV/C and the chemical potential μ. Performing a Bogoliubov transformation, we find equations for the particle and hole amplitudes u_n and v_n

$$\sum_j \begin{pmatrix} H_{ij} & \Delta_{ij} \\ \Delta^*_{ij} & -H_{ij} \end{pmatrix} \begin{pmatrix} u_n(j) \\ v_n(j) \end{pmatrix} = E_n \begin{pmatrix} u_n(i) \\ v_n(i) \end{pmatrix} \tag{6}$$

with

$$H_{ij} = \epsilon_i\delta_{ij} - t_{ij} \tag{7}$$

The self-consistency equation for the d-wave order parameter is then

$$\Delta_{ij} = \frac{V_{ij}}{2N_{\text{sc}}} \sum_{k_y}\sum_n \left[u_n(r_i)v^*_n(r_j)f(-E_n) - v^*_n(r_i)u_n(r_j)f(E_n)\right], \tag{8}$$

where $f(E)$ is the Fermi function and we use N_{sc} supercells in the direction parallel to the GB with the corresponding Bloch wave vector k_y. We adjust the chemical potential μ to ensure a fixed carrier density in the superconducting leads corresponding to 15% hole doping. The definition of the d-wave pair potential V_{ij} in the vicinity of the grain boundary is not straightforward since the bonds connecting a Cu to its neighbors are not exactly oriented

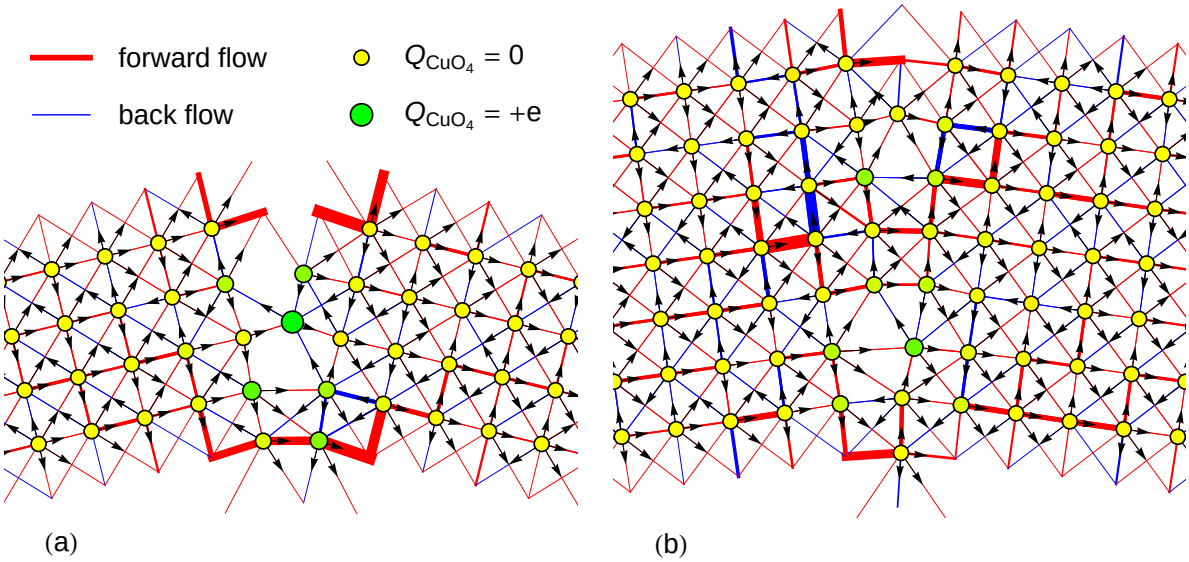

Figure 5: **Supercurrent distribution.** The current pattern in the vicinity of a (410) (a) and a (710) GB (b) calculated for $T \approx 0.25T_c$. The arrows only display the direction of the current, the red lines denote current flowing from left to right, blue lines denote current from right to left. The line thickness shows the current strength, while the point size and color of the Cu sites correspond to the on-site potential.

perpendicular to each other. We use a model that ties the strength of the pairing on a given bond to the size of the hopping on the bond, as well as to the charge difference across it, as detailed in the supplementary information. The final results for the critical current are not sensitive to the exact model employed.

With these preliminaries, the current itself can finally be calculated by imposing a phase gradient across the sample (see, e.g. Ref. 25 for details) from the eigenfunctions u_n, v_n and eigenvalues E_n of the BdG equations for the grain boundary,

$$\frac{j(r_i, r_j)}{e/\hbar} = -\frac{2it_{ij}}{N_{\rm sc}} \sum_{k_y} \sum_{n} [u_n^*(r_i)u_n(r_j)f(E_n) + v_n(r_i)v_n^*(r_j)f(-E_n) - \text{h.c.}] \qquad (9)$$

The critical current J_c is defined as the maximum value of the current as a function of the phase. In the tunnelling limit, when the barrier is large, this relationship is sinusoidal so the maximum current occurs at phase $\pi/2$. However, for very low angle grain boundaries we observe deviations from the tunnelling limit, i.e. higher transparency grain boundaries with non sinusoidal current-phase characteristics, although for the parameters studied here

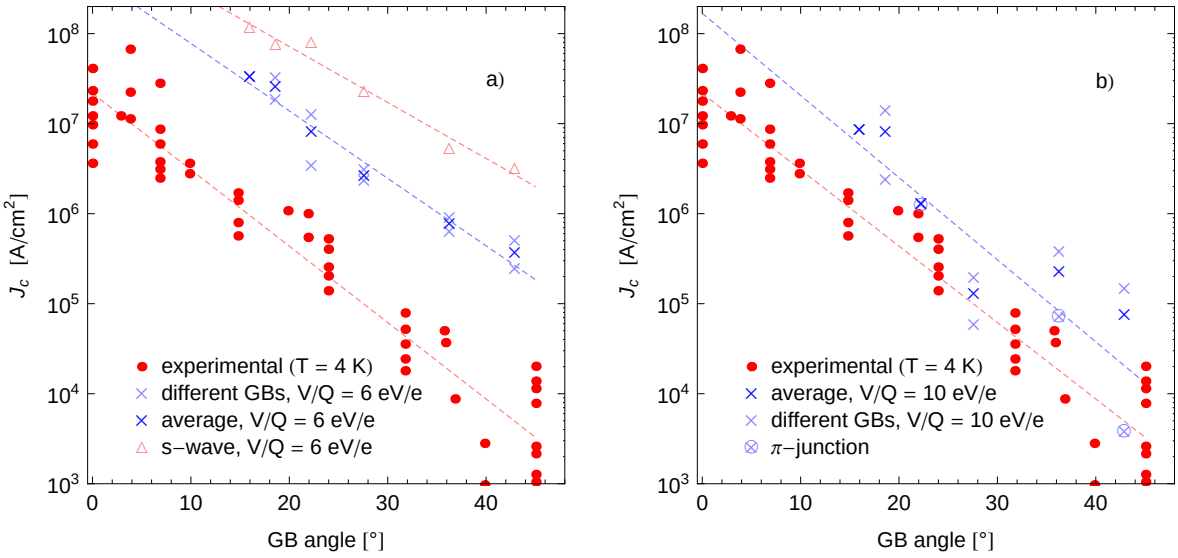

Figure 6: **Angle dependence of the critical current.** The critical current J_c as a function of the grain boundary angle α for screening lengths $\ell = 1.2$ Å (a) and 2 Å (b) calculated for $T \approx 0.25T_c$. Here the red points denote experimental results for YBCO junctions taken from Ref. 1, the light blue crosses show theoretical results for differently reconstructed GBs, the dark blue crosses show averaged theoretical values, and the light red triangles show "hypothetical" s-wave results. The dashed red and blue lines are exponential fits to the experimental and theoretical data, respectively.

these deviations are rather small.

It is instructive to examine the spatial pattern of supercurrent flow across a grain boundary, which is far from simple, as illustrated in Fig. 5. Along many bonds even away from the boundary, the current flows backwards or runs in closed loops around the squares. The flow appears to be dominated by large contributions between the regions which resemble classical dislocation cores. In most of our simulated grain boundaries we do not observe true π junction behavior, characterized by an overall negative critical current. To derive the total current density across a 2D cross section parallel to the grain boundary at $x = 0$ we sum up all contributions of $j(r_i, r_j)$ for which $x_i > 0$ and $x_j < 0$, with $x = 0$ the x coordinate (perpendicular to the interface) of the boundary, and normalize by the period length of the grain boundary structure $p = a/\sin\alpha$. We iterate the self-consistent solution until current conservation through every plane parallel to the GB is attained.

This calculation is in principle capable of providing the absolute value of the critical

current. To accomplish this, we have to normalize the current per grain boundary length by the height of the crystal unit cell c and multiply it by the number of CuO planes per unit cell $N_{\rm UC}$, e.g. for the YBCO compound under consideration $c = 11.7$ Å, $N_{\rm UC} = 2$,

$$j_c(x_0) = \frac{N_{\rm UC}}{pc} \sum_{i<j, x_i<0<x_j} j(r_i, r_j) \tag{10}$$

To account for the difference of the experimental gap magnitude from its calculated value (for numerical purposes chosen unrealistically large), we multiply the current by a factor of $\Delta_{\rm exp}/\Delta_0 = 25{\rm meV}/85{\rm meV}$, where $\Delta_{\rm exp}$ is the experimentally measured order parameter and Δ_0 is its self-consistently determined bulk value. We have checked that at the temperature the calculations have been performed ($T = 8{\rm meV} \approx 0.25 T_c$) an approximately linear scaling of the critical current as a function of the order parameter holds true for all grain boundary angles.

In Fig. 6, the critical current is plotted as a function of misorientation angle for a set of grain boundary junctions from (710) to (520) which we have simulated. All model parameters are fixed for the different junctions, except for a range of values affecting the initial conditions of the grain boundary reconstruction, which resulted in slightly different structures with the same misorientation angle α. Intriguingly, the variability of our simulated junctions is quite similar to the variability of actual physical samples as plotted in Fig. 6. For two different choices of the screening length ℓ, we see that the dependence on misorientation angle is exponential. Since in our picture this parameter directly affects the strength of the barrier, it is also natural that it should affect the exponential decay constant, as also shown by the Figure. The value of ℓ which gives the correct slope of the log plot yields a critical current which exceeds the experimental value by an order of magnitude. We speculate that the effect of strong correlations (see Ref. 26 and references therein), not yet included in this theory, may account for this discrepancy, given that a suppression by an order of magnitude was already shown for (110) junctions[9]. We show in addition results for "hypothetical" s-wave junctions using the same model parameters as for the d-wave junctions. We simply replaced the bond-centered pair potential by an on-site pair potential resulting in an isotropic s-wave state. Although it is one order of magnitude larger, the critical current for the s-wave junction still shows a similar exponential dependence on the grain boundary angle. We emphasize that this model does not reflect the situation in a "real" s-wave superconductor like niobium or lead, that do not show an exponential angle dependence of the grain boundary current,

since it is based on the microscopic structures of a CuO_2 plane.

Our detailed analysis of the grain boundary problem of HTS suggests that the primary cause of the exponential dependence on misorientation angle is the charging of the interface near defects which resemble classical dislocation cores[6], leading to a porous barrier where weak links are distributed in a characteristic way which depends on the global characteristics of the interface at a given angle (structure of defects, density of dislocations, etc.). The d-wave order parameter symmetry and the nature of the atomic wave functions at the boundary which modulate the hopping amplitudes do not appear to be essential for the functional form of the angle dependence although they cannot be neglected in a quantitative analysis. As such, we predict that this type of behavior may be observed in other classes of complex superconducting materials. Very recently, a report of similar tendencies in ferropnictide grain boundary junctions appeared to confirm this[27]. It will be interesting to use the new perspective on the longstanding problem to try to understand how Ca doping of the grain boundaries is able to increase the critical current by large amounts[28], and to explore other chemical and structural methods of accomplishing the same goal.

---

* Electronic address: siegfried.graser@physik.uni-augsburg.de

[1] Hilgenkamp, H. & Mannhart, J. Grain boundaries in high-T_c superconductors. *Rev. Mod. Phys.* **74**, 485-549 (2002).

[2] Dimos, D., Chaudhari, P., Mannhart, J. & LeGoues, F. K. Orientation dependence of grain-boundary critical currents in $YBa_2Cu_3O_{7-\delta}$ bicrystals. *Phys. Rev. Lett.* **61**, 219-222 (1988).

[3] Chaudhari, P., Dimos, D. & Mannhart, J. Critical Currents in Single-Crystal and Bicrystal Films. in *Earlier and Recent Aspects of Superconductivity* (eds Bednorz, J. G. & Müller, K. A.) 201-207 (Springer-Verlag, 1990).

[4] Sigrist, M. & Rice, T. M. Paramagnetic Effect in High T_c Superconductors - A Hint for d-Wave Superconductivity. *J. Phys. Soc. Jpn.* **61**, 4283-4286 (1992); *J. Low Temp Phys.* **95**, 389-393 (1994).

[5] Yokoyama, T., Sawa, Y., Tanaka, Y. & Golubov, A. A. Angular dependence of Josephson currents in unconventional superconducting junctions. *Phys. Rev. B* **75**, 020502(R) (2007).

[6] Gurevich, A., & Pashitskii, E. A. Current transport through low-angle grain boundaries in

high-temperature superconductors. *Phys. Rev. B.* **57**, 13878 (1998).

[7] Stolbov, S. V., Mironova, M. K. & Salama, K. Microscopic origins of the grain boundary effect on the critical current in superconducting copper oxides. *Supercond. Sci. Technol.* **12**, 1071-1074 (1999).

[8] Pennycook, S. J. *et al.* The Relationship Between Grain Boundary Structure and Current Transport in High-Tc Superconductors. in *Studies of High Temperature Superconductors: Microstructures and Related Studies of High Temperature Superconductors-II, Vol. 30* (ed Narlikar, A. V.) Ch. 6 (Nova Science Publishers, 2000).

[9] Andersen, B. M., Barash, Yu. S., Graser, S. & Hirschfeld, P. J. Josephson effects in *d*-wave superconductor junctions with antiferromagnetic interlayers. *Phys. Rev. B* **77**, 054501 (2008).

[10] Hu, C.-R. Midgap surface states as a novel signature for $d_{xa^2-xb^2}$-wave superconductivity. *Phys. Rev. Lett.* **72**, 1526-1529 (1993).

[11] Tanaka, Y. & Kashiwaya, S. Theory of Tunneling Spectroscopy of *d*-Wave Superconductors. *Phys. Rev. Lett.* **74**, 3451-3454 (1994).

[12] Löfwander, T., Shumeiko, V. S. & Wendin, G. Andreev bound states in high-T_c superconducting junctions. *Supercond. Sci. Technol.* **14**, R53-R77 (2001).

[13] Barash, Yu. S., Burkhardt, H. & Rainer, D. Low-Temperature Anomaly in the Josephson Critical Current of Junctions in *d*-Wave Superconductors. *Phys. Rev. Lett.* **77**, 4070-4073 (1996).

[14] Tanaka, Y. & Kashiwaya, S. Theory of the Josephson effect in *d*-wave superconductors. *Phys. Rev. B* **53**, 11957(R) (1996).

[15] Tanaka, Y. & Kashiwaya, S. Theory of Josephson effects in anisotropic superconductors. *Phys. Rev. B* **56**, 892 (1997).

[16] Zhang, X. & Catlow, C. R. A. Molecular dynamics study of oxygen diffusion in $YBa_2Cu_3O_{6.91}$. *Phys. Rev. B* **46**, 457 (1992).

[17] Phillpot, S. R. & Rickman, J. M. Simulated quenching to the zero-temperature limit of the grand-canonical ensemble. *J. Chem. Phys.* **97**, 2651-2659 (1992).

[18] Slater, J. C. & Koster, G. F. Simplified LCAO Method for the Periodic Potential Problem. *Phys. Rev.* **94**, 1498-1524 (1954).

[19] Harrison, W. A. Electronic structure and the properties of solids. (Dover Publications, 1989).

[20] Liu, P. & Wang, Y. Theoretical study on the structure of Cu(110)-p2×1-O reconstruction. *J. Phys.: Condens. Matter* **12**, 3955-3966 (2000).

[21] Baetzold, R. C. Atomistic Simulation of ionic and electronic defects in $YBa_2Cu_3O_7$. *Phys. Rev. B* **38**, 11304 (1988).

[22] Brown, I. D. A Determination of the Oxidation States and Internal Stress in $Ba_2YCu_3O_x$, x=6-7 Using Bond Valences. *J. of Solid State Chem.* **82**, 122-131 (1989).

[23] Chmaissem, O., Eckstein, Y. & Kuper, C. G. The Structure and a Bond-Valence-Sum Study of the 1-2-3 Superconductors $(Ca_xLa_{1-x})(Ba_{1.75-x}La_{0.25+x})Cu_3O_y$ and $YBa_2Cu_3O_y$. *Phys. Rev. B* **63**, 174510 (2001).

[24] Zhang, F. C. & Rice, T. M. Effective Hamiltonian for the superconducting Cu oxides. *Phys. Rev. B* **37**, 3759 (1988).

[25] Andersen, B. M., Bobkova, I., Barash, Yu. S. & Hirschfeld, P. J. $0-\pi$ transitions in Josephson junctions with antiferromagnetic interlayers. *Phys. Rev. Lett.* **96**, 117005-117008 (2006).

[26] Freericks, J. K. Transport in Multilayered Nanostructures. The Dynamical Mean-Field Theory Approach. (Imperial College Press, 2006).

[27] Lee, S. *et al.* Weak-link behavior of grain boundaries in superconducting $Ba(Fe_{1-x}Co_x)_2As_2$ bicrystals. *Appl. Phys. Lett.* **95**, 212505 (2009).

[28] Hammerl, G. *et al.* Possible solution of the grain-boundary problem for applications of high-T_c superconductors. *Appl. Phys. Lett.* **81**, 3209-3211 (2002).

Author Information

The authors declare no competing financial interests. Correspondence and requests for materials should be addressed to SG (siegfried.graser@physik.uni-augsburg.de).

Acknowledgments

This work was supported by DOE grant DE-FG02-05ER46236 (PJH), and by the DFG through SFB 484 and TRR 80 (SG, TK, RG, and JM) and a research scholarship (SG). We are grateful to Y. Barash for important early contributions to the project and we acknowledge fruitful discussions with A. Gurevich and F. Loder. PH would also like to thank the Kavli Institute for Theoretical Physics for support under NSF-PHY05-51164 during the writing of this manuscript. The authors acknowledge the University of Florida High-Performance

Computing Center for providing computational resources and support that have contributed to the research results reported in this paper.

Author contributions

R.G. applied the Slater-Koster technique to derive an effective tight-binding model Hamiltonian at the grain boundary and B.M.A. contributed in setting up the Bogoliubov-deGennes equations for the calculation of the critical current. S.G. carried out the numerical calculations under the supervision of P.J.H. and T.K.. J.M. contributed with his experience and knowledge about grain boundaries and the physical lengthscales involved. All authors contributed to the analysis of the results. P.J.H., T.K., J.M., and S.G. wrote the manuscript.

Figure 1: Schematic of an HTS symmetric grain boundary. The misorientation angle α and the orientation of the d-wave order parameters are indicated.

Figure 2: Top view of a calculated (410) grain boundary. Here only the Y and the CuO_2 layers are shown. The dots show the position of Y ions (magenta), Cu ions (yellow), and O ions (red). Structural units are indicated by solid black lines. For this particular angle we find a sequence of the form A(A/2)B#(A/2)B, in agreement with the experimental results given in Table 1 of Ref. 8 (for notation see this reference).

Figure 3: Tight-binding model for the CuO_2 plane. Hopping values between the Cu ions calculated from the interatomic matrix elements for a (410) grain boundary (a) and for a (710) grain boundary (b). The line thickness and line colors characterize the hopping amplitudes (blue: weak, red: strong) and the color and size of the copper sites illustrate the on-site potential.

Figure 4: Supercurrent distribution. The current pattern in the vicinity of a (410) (a) and a (710) GB (b) calculated for $T \approx 0.25T_c$. The arrows only display the direction of the current, the red lines denote current flowing from left to right, blue lines denote current from right to left. The line thickness shows the current strength, while the point size and color of the Cu sites correspond to the on-site potential.

Figure 5: Angle dependence of the critical current. The critical current J_c as a function of the grain boundary angle α for screening lengths $\ell = 1.2$ Å (a) and 2 Å (b) calculated for $T \approx 0.25T_c$. Here the red points denote experimental results for YBCO junctions taken from Ref. 1, the light blue crosses show theoretical results for differently reconstructed GBs, the dark blue crosses show averaged theoretical values, and the light red triangles show "hypothetical" s-wave results. The dashed red and blue lines are exponential fits to the experimental and theoretical data, respectively.